


# Effect of Test Setups on the Shear Transfer Capacity Across Cracks in FRC

**Conference Paper****Author(s):**

Giraldo Soto, Alejandro; Kaufmann, Walter 

**Publication date:**

2020

**Permanent link:**

<https://doi.org/10.3929/ethz-b-000453091>

**Rights / license:**

[In Copyright - Non-Commercial Use Permitted](#)

**Originally published in:**

RILEM Bookseries 30, [https://doi.org/10.1007/978-3-030-58482-5\\_15](https://doi.org/10.1007/978-3-030-58482-5_15)

## EFFECT OF TEST SETUPS ON THE SHEAR TRANSFER CAPACITY ACROSS CRACKS IN FRC

A. Giraldo Soto <sup>(1)\*</sup> and W. Kaufmann <sup>(1)</sup>

<sup>(1)</sup> Chair of Concrete Structures and Bridge Design, Institute of Structural Engineering, ETH Zürich, Switzerland

\* Corresponding author: [giraldo@ibk.baug.ethz.ch](mailto:giraldo@ibk.baug.ethz.ch)

### ABSTRACT

The shear transfer capacity of concrete across cracks is highly relevant in situations where the principal concrete stress directions are not aligned with the cracks. Fibres are effective in controlling the crack opening, thereby enhancing aggregate interlock and hence, the ability of transferring shear stresses across cracks. Compared to plain concrete, higher stresses can therefore be transferred across cracks in fibre reinforced concrete (FRC). However, the shear transfer across cracks in FRC has received much less attention over the past decades than the residual tensile stress transfer across orthogonally opening cracks, and no generally accepted model for this behaviour is available today. The shear transfer capacity and the calibration of most existing models are obtained from experimental tests which presume failures occurring in “pure shear”, being the most popular used test setups: (i) Z-type push-off specimen; (ii) modified JSCE-G 553; and (iii) FIP shear test method (asymmetrical four-point bending). However, significant differences have been observed in the experimental resulting shear strength, depending on the test setup. These differences have not been evaluated systematically until now. In order to address this issue, the authors carried out an experimental campaign on specimens made from identical SFRC mixes with varying fibre dosage, testing each mix in all three mentioned setups. The paper presents the results of this experimental campaign.

**KEYWORDS:** steel fibre reinforced concrete, shear transfer, interface shear, experimental testing, push-off test, JSCE shear test, FIP shear test, cracks, crack kinematics, aggregate interlock, shear test setup.

### 1. INTRODUCTION

Contrary to the residual tensile stresses in orthogonally opening cracks in fibre reinforced concrete (FRC), the transfer of shear stresses across cracks in FRC has received only limited attention over the past decades, and no generally accepted model is available for the case of skew crack opening in FRC. However, this is highly relevant in situations where the principal concrete stress directions are not aligned with the cracks, such as in orthotopically reinforced panels and webs of girders. In such elements, the principal concrete compressive stress direction rotates towards the stronger reinforcement after the onset of yielding, causing substantial deviations from the direction of initial cracks.

Furthermore, cracks deviating from the principal compressive stress direction may be caused by restrained shrinkage or previous, non-proportional loading.

Fibres are effective in controlling the crack opening, thereby enhancing aggregate interlock and hence, the ability of transferring shear stresses across cracks. Compared to plain concrete, higher stresses can therefore be transferred across cracks in fibre reinforced concrete.

Different experimental setups have been used in the past to examine the shear transfer across cracks in FRC [1]–[11]. While apparently simple to conduct, such experiments are demanding since large forces are required, and very small displacements of the irregular crack faces need to be controlled and measured. The state of stress in the interface is hardly ever uniform, even in complex experimental setups, due to the irregularity of the crack faces and the difficulty of generating shear without concomitant bending moments. In addition, the fibre distribution and orientation in the interface are also subject to variations. Hence, test results are subject to considerable scatter. Furthermore, a recent study aimed at establishing a mechanical model for the shear transfer across cracks in FRC, relating the shear and normal stresses to the crack kinematics, i.e. crack opening and slip [12], identified substantial differences in the results obtained from different experimental setups used for determining the “shear strength” of FRC.

In order to address this issue, the authors carried out an experimental campaign on specimens made from identical SFRC mixes, tested in three different setups adopted in previous experimental studies investigating the “shear strength” of FRC, illustrated in Figure 1: (a) Z-type push-off tests as known from classic investigations of aggregate interlock in plain and reinforced concrete [13]–[18]; (b) modified JSCE-G 553 shear tests [19]; and (c) FIP shear tests [20]. More details on the test setups and specimen geometry are given in Section 2.

## 2. EXPERIMENTAL CAMPAIGN

In order to study the test setups effect on the shear transfer capacity across cracks in SFRC, three different, existing experimental test setups (Z-type push-off, modified JSCE-G 553 and FIP shear tests), used to determine the shear resistance in plain concrete and fibre reinforced concrete, are carried out. For this purpose, the specimens of each type of test are made with the same concrete mixture using different amounts of steel fibres: 0 kg/m<sup>3</sup>, 40 kg/m<sup>3</sup>, 60 kg/m<sup>3</sup> and 80 kg/m<sup>3</sup> (0%, 0.5%, 0.75%, 1%). Therefore, a total of 12 shear tests, 4 tests for each test setup (3x4), were conducted. Table 1 identifies the tests and specimens.

**Table 1.** Tests and specimen identification.

Z-Type	Specimen ID		$\rho_f$ [%]	[kg/m <sup>3</sup> ]
	JSCE	FIP		
Z-0	JSCE-0	FIP-0	0.00	0
Z-40	JSCE-40	FIP-40	0.50	40
Z-60	JSCE-60	FIP-60	0.75	60
Z-80	JSCE-80	FIP-80	1.00	80

### 2.1. Experimental setups and specimen geometry

The experimental shear test setups and the geometry of the specimens are shown in Figure 1.

The Z-Type push-off specimens (Figure 1a) consist of two reinforced L-shaped blocks that are 300 mm wide, 474 mm high and 150 mm deep. In order to avoid cracking outside the intended failure plane, a 15 mm deep and 2.5 mm wide notch was sawed on the front and rear of the specimens. The shear plane has a theoretical area of 120x120 mm (14'400 mm<sup>2</sup>). The support and the applied load  $F$  are vertically aligned in the specimen axis, having a width of 60 mm. The average shear stress  $\tau$  in the shear plane is calculated as  $\tau = F/A_c$ , where  $A_c$  is the area of the shear plane.

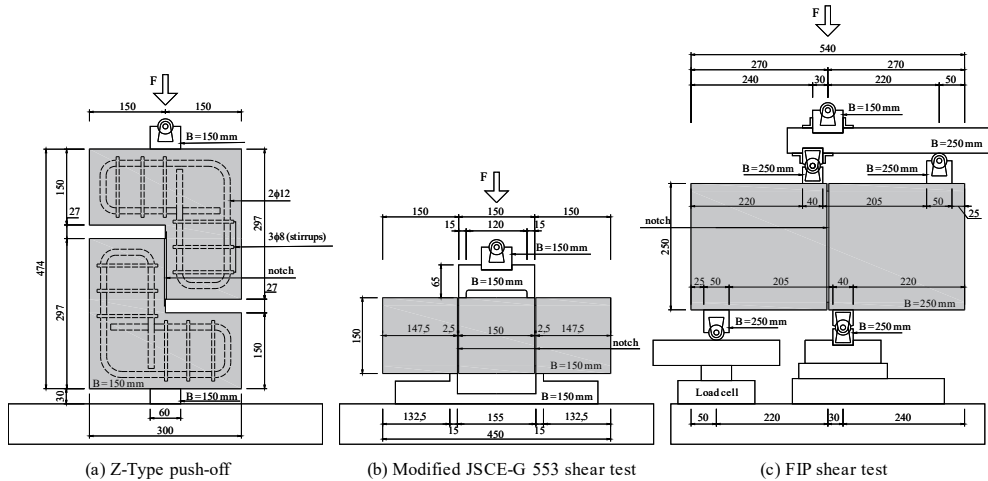


**Figure 1.** Shear test setups and geometry of the specimens.

The modified JSCE-G 553 (Figure 1b) is a modified version of the standardized shear test JSCE-G 553-2010 [19], specified by the Japanese Society of Civil Engineering (JSCE), where notches in the two shear planes are included. The specimen consists of a square prism of 450 mm length, with a square cross-section of 150 mm side length. This test is composed of two shear planes, and to avoid cracking outside these intended failure shear planes, a 15 mm deep and 2.5 mm wide notches were sawed all around the specimen. The theoretical total area of both shear planes is twice  $120 \times 120 \text{ mm}$  ( $2 \times 14'400 = 28'800 \text{ mm}^2$ ). The specimen is supported by two relatively small bearing surfaces of 15 mm width, located just outside of the notches. The load  $F$  is applied symmetrically on the specimen, acting over a width of 15 mm located on the inner side near the shear planes. The average shear stress  $\tau$  in the shear plane is calculated as  $\tau = F/A_c$ , where  $A_c$  is the sum of the area of both shear planes. Note that due to the geometric configuration of the test – which can be seen as a four-point-bending test with short shear span – the shear stress  $\tau$  is always accompanied by a normal stress  $\sigma \approx 0.1 \tau$  (if loads and reactions act centric on the loading plates), and furthermore, the relevant sections are subject to global bending, which accumulates compression stresses in the upper part.

The FIP standard shear test (Figure 1c) is performed according to the FIP report published in 1978 [20]. The FIP specimen consists of a square prism of 540 mm length, with a square cross-section of 250 mm side length. In order to avoid cracking outside the intended failure shear plane, a 15 mm deep and 2.5 mm wide notch was sawed all around the specimen, which leads to a theoretical shear area of  $220 \times 220 \text{ mm}$  ( $48'400 \text{ mm}^2$ ). The specimen is loaded in asymmetrical four-point bending by means of a sophisticated arrangement of steel elements used to introduce the load  $F$  (the load axis coincides with the shear plane in the middle of the specimen) and to support the sample. The shear force  $V$  acting in the shear plane is equal to  $V = F \cdot (220 - 30)/(220 + 30) = 0.76 \cdot F$ , therefore the average shear stress  $\tau$  in the shear plane is calculated as  $\tau = 0.76 \cdot F/A_c$ , where  $A_c$  is the area of the shear plane.

## 2.2. Equipment and tests procedure

The tests are carried out using a Servohydraulic Universal Testing Machine with a maximum capacity of 1600 kN. The crack and the relative displacements of the shear planes were measured by two different optical measuring systems. Digital Image Correlation (DIC) was used in the front face and the laser scanning, NDI system, in the rear face. In addition, a load cell with 200 kN capacity was used for the FIP test setup in order to measure and control the reaction on one of the two bearings (Figure 1c),

especially in the post-cracking state where certain eccentricities may be caused by displacements of the specimen.

### 2.2.1. Digital Image Correlation (DIC)

The DIC measurement system (Figure 2) used consisted of two Prosilica GT600 29MPx cameras (with Rodagon lenses,  $f=80$  mm). The distance between the cameras and the test specimens varied between 1.6 m and 2 m and the frequency of image capture was 2 Hz. The dot size of the speckle pattern used on the samples was 0.66 mm (Figure 2).

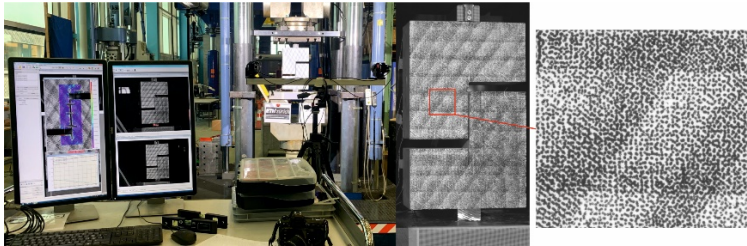


**Figure 2.** Overview of the DIC measurement system and speckle pattern with dots of 0.66 mm.

### 2.2.2. Laser scanning, NDI system

An optical measurement system NDI was used to measure the displacements on the rear face of the specimens. Figure 3 shows the optical sensors attached to the specimens; all of them were tracked with a frequency of 50 Hz. The sensors around the notch can capture the initiation and propagation of the crack and the other sensors serve as reference points and allow information about rotational movements to be obtained.

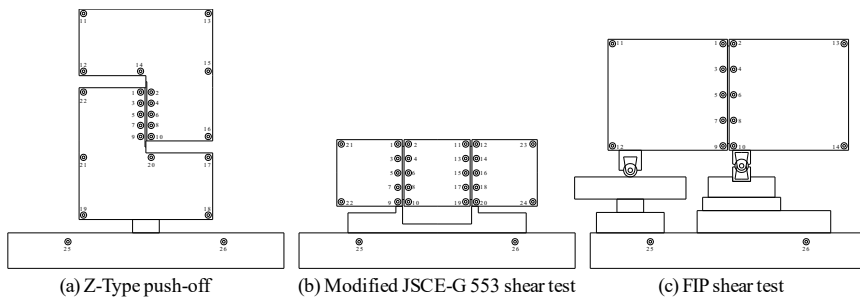


**Figure 3.** Optical sensors on the rear face of the specimens.

### 2.2.3. Test procedure

In order to take into account the softening behaviour of the SFRC, the load on the specimens is applied in displacement control, and two load phases were considered. The first load phase was running with a displacement rate of 0.06 mm/min until a displacement of 1 mm after the peak (the peak is detected by a load drop of 3 kN) was achieved. Once the first load phase is concluded, continuously the second load phase is started with a displacement rate of 0.5 mm/min until the relative displacement reaches 15 mm (see Table 2 and Figure 4).

**Table 2.** Displacement ratio of the applied load phases.

	Phase 1	Phase 2
Displacement rate [mm/min]	0.06	0.50

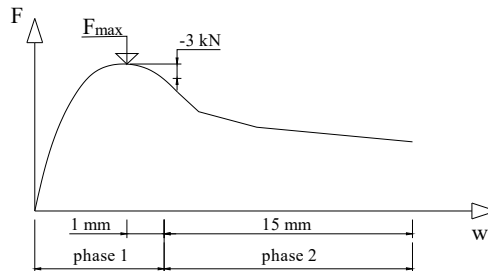


Figure 4. Load application criteria for phase 1 and 2.

### 2.3. Materials and concrete mix

All specimens were made from identical SFRC mixes with four different fibre dosages: 0 kg/m<sup>3</sup>, 40 kg/m<sup>3</sup>, 60 kg/m<sup>3</sup> and 80 kg/m<sup>3</sup> (0%, 0.5%, 0.75%, 1%), using a concrete mix (Table 3) suited to obtain a normal strength concrete C30/37. Industry-standard Dramix 3D 80/50BG steel fibres were used, whose geometry and material properties are shown in Table 4.

Table 3. Mixture composition and properties of the concrete.

Mixture constituent			Concrete properties <sup>1)</sup>			
Cement 42.5	384	[kg/m <sup>3</sup> ]	$\rho_f$ [%]	Days <sup>2)</sup>	$f_c$ [MPa]	$E_c$ [GPa]
Water	204	[kg/m <sup>3</sup> ]	0.00	28	37.1	-
Sand	939	[kg/m <sup>3</sup> ]	0.00	72	43.9	30.2
Aggregate 4-8 mm	816	[kg/m <sup>3</sup> ]	0.50	72	-	-
Additive	0	[kg/m <sup>3</sup> ]	0.75	72	42.4	30.4
W/C	53	[%]	1.00	72	42.4	30.2
Fibres 80/50BG	0-40-60-80	[kg/m <sup>3</sup> ]	<sup>1)</sup> Standard concrete cylinder test.			

<sup>2)</sup> Shear tests: 72 days.

Table 4. Steel fibres geometry and material properties.

Geometry			Material properties		
Fibre family	3D	[-]	Nom. tensile strength	1'270	[N/mm <sup>2</sup> ]
Length	50	[mm]	Modul of elasticity	200'000	[N/mm <sup>2</sup> ]
Diameter	0.62	[mm]	Strain at ultimate strength	0.8	[%]
Aspect ratio	80	[-]			

### 2.4. Experimental results

The maximum average shear stress capacity  $\tau_{max}$  for each specimen, considering the effective shear plane areas ( $A_{c,eff}$ ), are shown in Table 5. For a proper interpretation of the results, it is essential to know the effective (real) fibre volume fraction  $\rho_{f,eff}$  in the shear plane, which may differ from the theoretical fibre volume fraction (0%, 0.5%, 0.75% and 1%), due to the non-homogeneous 3D distribution and orientation of fibres produced by the phenomenon known as *wall effect* or by obstruction of reinforcements concentrated in certain areas. In order to address this issue, the effective fibre volumetric fractions  $\rho_{f,eff}$  in the shear plane of the specimens have been determined by counting the number of fibres in the crack plane  $N_f$ . However, it is not entirely accurate to visually quantify the effective volumetric fraction in the shear plane, due to (i) the difficulty in counting fibres (some of them are broken and others are slipped), and (ii) the theoretical assumption which refers to a homogeneous 3D fibre distribution and orientation. The total number of fibres counted in the shear plane are divided by the theoretical 3D fibre orientation factor  $K_{f(3)} = 0.5$  [21]. The effective fibre volume fractions  $\rho_{f,eff}$  in the shear plane of the specimens and the shear test results versus theoretical and effective fibre

volume fraction plots are shown in Table 5 and Figure 5, respectively. As shown Table 5, the effective volumetric fibre contents  $\rho_{f,eff}$  in the shear plane vary from the theoretical values  $\rho_f$  by -8% to +12% in the Z-type test and by -33% to -16% in the JSCE and FIP tests.

Regarding Specimen Z-40 ( $\rho_f = 0.5\%$ ), its maximum average shear stress is closer to the shear resistance of the plain concrete specimen Z-0 (difference less than 10%), which indicates that the fibres have not had a significant influence on the maximum shear resistance. This issue can be attributed to the non-homogeneous distribution of the fibres in the shear plane, which were concentrated mainly in the edges, thus producing in the central area, where the highest shear stresses should be transferred (see Figure 6a and Figure 6b), a zone practically free of fibres (see Figure 6c).

**Table 5.** Maximum average shear stresses capacity ( $f_{c,test day} = 43 \text{ N/mm}^2$ ).

Specimen ID	$\rho_f$ [%]	$N_f$ [-]	$\rho_{f,eff}$ [%]	$\frac{\rho_{f,eff}}{\rho_f}$	$F_{max}$ [kN]	$A_{c,eff}$ [mm <sup>2</sup> ]	$\tau_{max}$ [N/mm <sup>2</sup> ]
Z-0	0.00	0.00	0.00	-	79	13'800	5.7
Z-40	0.50	135	0.56	1.12	92	14'760	6.2
Z-60	0.75	163	0.69	0.92	131	14'520	9.0
Z-80	1.00	242	1.03	1.03	148	14'400	10.3
JSCE-0	0.00	0.00	0.00	-	182	27'848	6.5
JSCE-40	0.50	96	0.42	0.84	220	27'848	7.9
JSCE-60	0.75	122	0.54	0.72	246	27'966	8.8
JSCE-80	1.00	189	0.82	0.82	275	28'321	9.7
FIP-0	0.00	0.00	0.00	-	269	49'506	4.1
FIP-40	0.50	332	0.42	0.84	367	48'730	5.7
FIP-60	0.75	440	0.53	0.71	427	48'840	6.6
FIP-80	1.00	533	0.67	0.67	457	48'841	7.1

Figure 5 shows that the shear stress capacity increases approximately linearly with the steel fibre content, and the trendlines of the test results per setup (Figure 5b) are nearly parallel. From the latter, it can be concluded that the test configuration had a similar influence on the shear capacity, independently of the fibre volume (note that Z-40 specimen test result (Z-type push-off) is excluded from the trendline for the reasons outlined above).

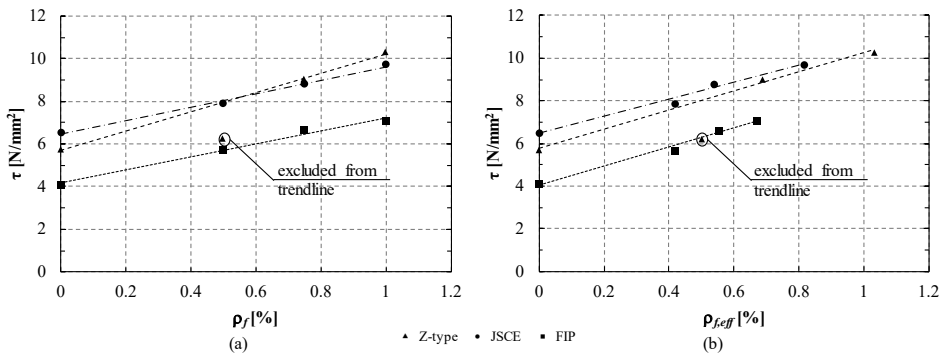


**Figure 5.** (a) Shear test results – theoretical fibre volume fraction. (b) Shear test results – effective fibre volume fraction.

Considering the Z-type tests results as reference (Figure 5b) – as explained below, this test setups should theoretically be the most reliable to determine the shear transfer capacity –, the experimental shear



capacities obtained by JSCE and FIP tests setups are around 6% higher and 20% lower, respectively. These differences can be attributed to the test setups. The FIP test setup (asymmetrical four-point bending test) produces tensile stresses in the upper and lower part of the specimen (according to a strut-and-tie model and confirmed by the DIC measurements, see Figure 7a and Figure 7b). These tensile stresses cause a premature failure of the specimen in comparison with the other two test setups; in fact, the plain concrete specimen did not fail in the expected shear plane despite the notch that had been sawed all around the specimen (Figure 7c and Figure 7d).

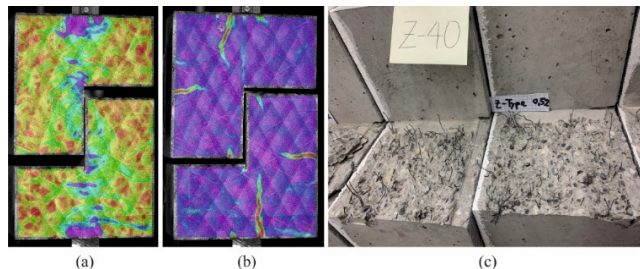


**Figure 6.** Z-Type specimens. (a) Minimum principal strain of Z-60 test (DIC capture). (b) Failure of specimen Z-60 (DIC capture). (c) Fibre distribution in share plane of Z-40 after test.

The higher nominal shear stresses obtained in the JSCE tests are attributed to the beneficial compressive stresses produced by the *arching effect*, which is expected due to the test setup and confirmed by the DIC measurements (Figure 8a). The narrow bearing surfaces, subject to high vertical stresses, can resist high horizontal reactions resulting from the test setup (the specimen tends to extend at the bottom), which avoids horizontal tensile stresses at the bottom of the specimen necessary for equilibrium with the compression in the upper part. On the other hand, due to the high stresses concentrations, the contact surfaces are prone to fail and consequently, negatively affect the maximum load capacity. In fact, Specimens JSCE-40 and JSCE-80 failed by local indentation of the contact surfaces, see below (Figure 8b and Figure 8d).

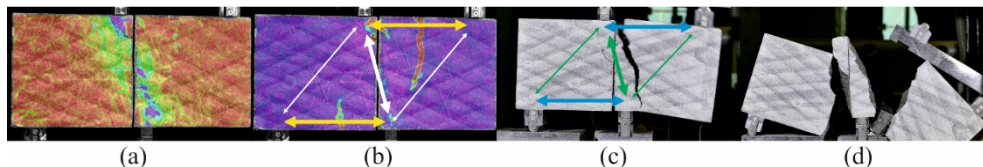


**Figure 7.** DIC captures of FIP tests. (a) Minimum principal strain of FIP-80 test. (b) Maximum principal strain of FIP-80 test. (c) and (d) Failure of the plain concrete specimen of FIP-0 test.

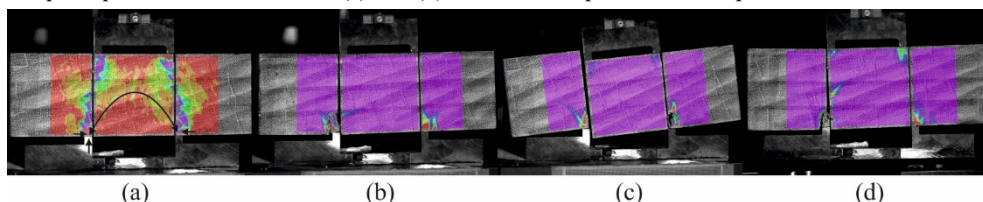


**Figure 8.** DIC captures of JSCE tests. (a) Arching effect. (b) Failure of specimen JSCE-40. (c) Failure of specimen JSCE-60. (d) Failure of specimen JSCE-80.

No particularities that could significantly have affected the shear transfer were observed in the Z-type push-off tests (see Figure 6a and Figure 6b). Therefore, the authors consider that the results obtained with the Z-Type test setup give the most reliable results among the three test setups studied. The shear stress - crack width and shear stress - slip curves for all tests are shown in Figure 9. The crack kinematics



was calculated as the average of the relative displacements along the vertical crack, at both sides of the specimen (front and rear), which were obtained by the DIC measurement system on the front side and by the NDI measurement system on the rear side.

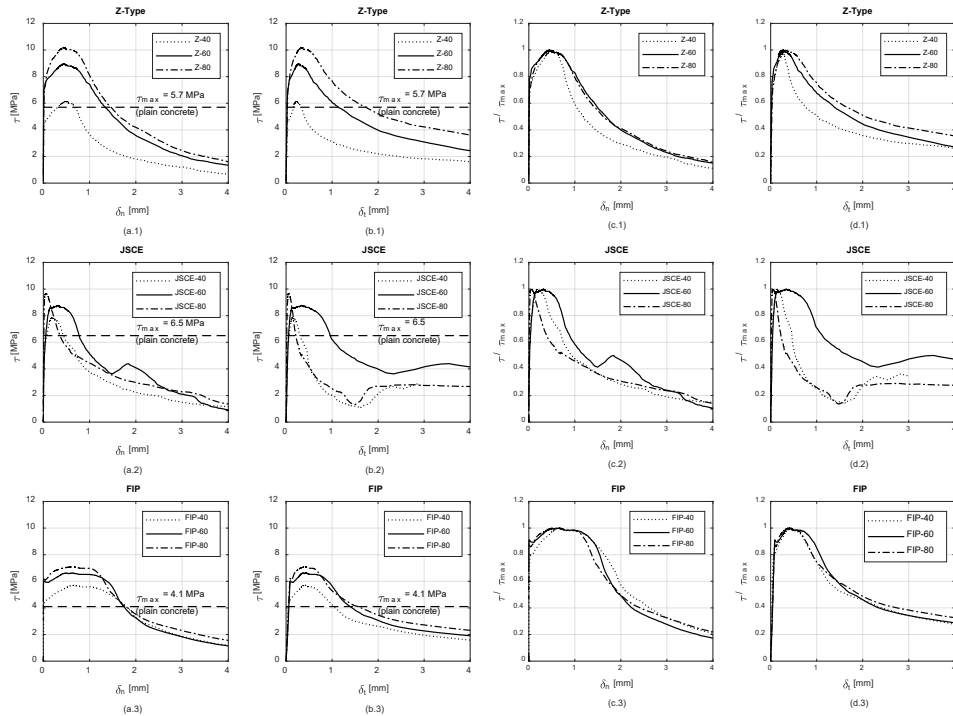


**Figure 9.** (a) Shear stress  $\tau$  – crack width  $\delta_n$ . (b) Shear stress  $\tau$  – crack slip  $\delta_i$ . (c) Shear stress to max. shear stress ratio  $\tau/\tau_{max}$  – crack width  $\delta_n$ . (d) Shear stress to max. shear stress ratio  $\tau/\tau_{max}$  – crack slip  $\delta_i$ . Comparing the curves for the different fibre volume fractions, it can be seen that the curves of the Z-Type (Figure 9c.1 and Figure 9d.1) and FIP (Figure 9c.3 and Figure 9d.3) test setups are fairly congruent; particularly the FIP tests exhibit quite similar load-average crack kinematics curves. It is also observed that at equal ratios  $\tau/\tau_{max}$ , larger average crack widths and slips are observed in the FIP tests, and that at the same average crack opening, higher ratios  $\tau/\tau_{max}$  are observed in these tests (e.g. for  $\delta_n = 1\text{ mm}$ , the ratios  $\tau/\tau_{max}$  for Z-60, JSCE-60 and FIP-60 are around 0.82, 0.58 and 0.97, respectively). This can be explained by the tensile stress fields produced by the test setup (discussed above), tending to increase the crack opening in the shear plane. Regarding the JSCE test, since the *arching effect* (discussed above) causes compressive stresses in the shear plane, the maximum shear capacity  $\tau_{max}$  should be higher, and the crack opening and slip in the shear plane tend to be less than the other setups. However, the shear failures in these tests occurred in combination with local concrete failures at the supports (see Figure 8b and Figure 8d). The failures at the supports were dominant in the JSCE-40 and JSCE-80 tests, while a shear failure was observed for JSCE-60 test (see Figure 8c). This explains why average crack width and slip curves of the specimen JSCE-60 have a smoother softening behaviour than the JSCE-40 and JSCE-80 specimens (Figure 9a.2 to Figure 9d.2), which exhibit a very pronounced softening after the maximum load is reached (just when the concrete supports failed, as confirmed by the DIC images). However, it cannot be concluded how much influence this combined

failure had on the maximum shear stress capacity because both the JSCE-40 and JSCE-80 specimens and the JSCE-60 fit the trendline (Figure 5b).

## 11. CONCLUSIONS

From the considerations of the previous paragraphs the following main conclusion can be drawn:

- The shear capacity depends on the stress state in the shear plane, which is not homogeneous in reality, and accompanied by normal stresses depending on the test setup which also influence the crack opening. The test setups therefore clearly bias the measured shear transfer capacity across the crack. In this respect, no particularities were observed in the Z-type test setup that could significantly affect the shear transfer capacity. The authors therefore consider this test setup as the most reliable of the three tests studied to determine the shear transfer capacity.
- In the modified JSCE-G 553 tests, the shear transfer capacity is clearly affected by an *arching effect* (Figure 8a), which compresses the shear plane and reduces the crack opening. Consequently, this setup tends to overestimate the shear capacity. The experimental shear capacities observed in the JSCE test setup carried out by the authors were only approximately 6% higher than those obtained by the Z-type tests due to local failures at the bearing surfaces. However, due to the *arching effect* and the kinematics of the specimen after cracking (Figure 8c), further modifications on the JSCE-G 553 (or previous version JSCE-SF 6 [22]) shear test to avoid such failures, e.g. by providing additional supports at the ends of the specimen [8], favour the formation of the arc effect by increasing the normal compressive stresses and, accordingly, lead to a much more pronounced overestimation of the shear transfer capacity. This explains the much higher shear transfer capacities observed using such setups [8], as observed by [12].
- The FIP test setup causes tensile stresses in the upper and lower part of the specimen (Figure 7a and Figure 7b), which cause a premature failure of the specimen and thus lower shear transfer capacities compared to the other two shear test setups. Therefore, the FIP shear test setup underestimated the shear transfer capacity by approx. 20% compared to the Z-type test setup.
- The authors are not aware of any specific study in the literature regarding the influence of the stress state in the shear plane, produced by the test setups, on the shear transfer capacity. Neglecting this clearly significant influence of the test setup partly explains the wide variation in the predictions of the shear transfer capacity obtained from empirical models, which were calibrated using different test setups. The comparison of the experimental results with theoretical models underlying this conclusion will be published in a separate paper.
- The results show that the shear transfer capacity increases approximately linearly with the steel fibre volume fraction, and the trendlines of the test setup results (Figure 5b) tend to be parallel to each other.
- Due to the non-homogeneous 3D distribution and orientation of fibres produced by the phenomenon known as *wall effect* or by obstruction of reinforcements concentrated in certain areas, the effective fibre volumetric fractions  $\rho_{f,eff}$  in the shear plane differ from the theoretical fibre volume fractions  $\rho_f$ , where in some cases the differences are significant, with up to 33% deviation in the tests.

## ACKNOWLEDGEMENTS

The support of Patrick Studer and Yanik Pfister in carrying out the experimental campaign and post-processing the results, as part of their MSc Project at ETH Zurich, is greatly acknowledged.

## REFERENCES

- [1] J. Jayaprakash, A. A. Abdul Samad, and A. Abbasvoch, "Experimental Investigation on Shear Capacity of Reinforced Concrete Precracked Push-off Specimens with Externally Bonded Bi-Directional Carbon Fibre Reinforced Polymer Fabrics," *Mod. Appl. Sci.*, vol. 3, 2009, doi: 10.5539/mas.v3n7p86.
- [2] A. R. Khaloo and N. Kim, "Influence of concrete and fiber characteristics on behavior of steel fiber reinforced concrete under direct shear," *ACI Mater. J.*, vol. 94, no. 6, pp. 592–601, 1997.
- [3] B. Boulekbache, M. Hamrat, M. Chemrouk, and S. Amziane, "Influence of yield stress and compressive strength on direct shear behaviour of steel fibre-reinforced concrete," *Constr. Build. Mater.*, vol. 27, no. 1, pp. 6–14, 2012, doi: <https://doi.org/10.1016/j.conbuildmat.2011.07.015>.
- [4] M. Mostafazadeh and A. Abolmaali, "Shear Behavior of Synthetic Fiber Reinforced Concrete," *Adv. Civ. Eng. Mater.*, vol. 5, pp. 371–386, 2016, doi: 10.1520/ACEM20160005.
- [5] A. Khanlou, G. A. MacRae, A. N. Scott, S. J. Hicks, and G. C. Clifton, "Shear performance of steel fibre-reinforced concrete," presented at the Steel Innovations Conference 2013, Christchurch, New Zealand, 2013, pp. 21–22.
- [6] Amir A. Mirsayah and Nemkumar Banthia, "Shear Strength of Steel Fiber-Reinforced Concrete," *ACI Mater. J.*, vol. 99, no. 5, Sep. 2002, doi: 10.14359/12326.
- [7] M. A. Mansur, T. Vinayagam, and K.-H. Tan, "Shear transfer across a crack in reinforced high-strength concrete," *J. Mater. Civ. Eng.*, vol. 20, no. 4, pp. 294–302, 2008, doi: 10.1061/(ASCE)0899-1561(2008)20:4(294).
- [8] T. Soetens and S. Matthys, "Shear-stress transfer across a crack in steel fibre-reinforced concrete," *Cem. Concr. Compos.*, vol. 82, pp. 1–13, 2017, doi: <https://doi.org/10.1016/j.cemconcomp.2017.05.010>.
- [9] G. Appa Rao and A. Sreenivasa Rao, "Toughness indices of steel fiber reinforced concrete under mode II loading," *Mater. Struct.*, vol. 42, no. 9, p. 1173, Aug. 2009, doi: 10.1617/s11527-009-9543-6.
- [10] E. Cuenca and P. Serna, "Shear Behavior of Self-Compacting Concrete and Fiber-Reinforced Concrete Push-Off Specimens," in *Design, Production and Placement of Self-Consolidating Concrete*, Dordrecht, 2010, pp. 429–438.
- [11] B. Li, K. Maekawa, and H. Okamura, "Contact density model for stress transfer across cracks in concrete," *J. Fac. Eng.*, vol. 40, no. 1, pp. 9–52, 1989.
- [12] W. Kaufmann, A. Amin, A. Beck, and M. Lee, "Shear transfer across cracks in steel fibre reinforced concrete," *Eng. Struct.*, vol. 186, pp. 508–524, 2019, doi: <https://doi.org/10.1016/j.engstruct.2019.02.027>.
- [13] Mariano Valle and Oral Buyukozturk, "Behavior of Fiber Reinforced High-Strength Concrete Under Direct Shear," *ACI Mater. J.*, vol. 90, no. 2, Mar. 1993, doi: 10.14359/4006.
- [14] L. Van De Loock, "Influence of steel fibres on the shear transfer in cracks," in *Proc. Int. Symp. Fibre Reinf. Concr.*, Madras, India, 1987, pp. 1101–1112, [Online]. Available: <https://www.scopus.com/record/display.uri?eid=2-s2.0-85062080024&origin=inward>.
- [15] W. Kaufmann, *Strength and deformations of structural concrete subjected to in-plane shear and normal forces*. 1998.
- [16] Z. P. Bazant and P. Gambarova, "Rough cracks in reinforced concrete," *ASCE J Struct Div*, vol. 106, no. 4, pp. 819–842, 1980.
- [17] J. C. Walraven, "Fundamental analysis of aggregate interlock," *ASCE J Struct Div*, vol. 107, no. 11, pp. 2245–2270, 1981.
- [18] B. Li and K. Maekawa, "Contact density model for cracks in concrete," *LABSE*, vol. 54, pp. 51–62, 1987, doi: <https://doi.org/10.5169/seals-41916>.
- [19] Japan Society of Civil Engineers (JSCE), *JSCE-G 553 Test method for shear strength of steel fiber reinforced concrete*. 2010.

- [20] Fédération Internationale de la Précontrainte, “Technical reoport: Shear at the interface of precast and in situ concrete,” 1978.
- [21] T. Pfyl, “Tragverhalten von Stahlfaserbeton,” Swiss Federal Institute of Technology in Zurich, 2003.
- [22] Japan Society of Civil Engineers (JSCE), *JSCE-SF 6 Method of test for shear strength of steel fiber reinforced concrete*. 1990.